Contrasting microfossil preservation and lake chemistries within the 1200–1000 Ma Torridonian Supergroup of NW Scotland

DAVID WACEY[1,2]*, MARTIN BRASIER[3]†, JOHN PARNELL[4], TIMOTHY CULWICK[3], STEPHEN BOWDEN[4], SAM SPINKS[5], ADRIAN J. BOYCE[6], BRETT DAVIDHEISER-KROLL[6], HEEJIN JEON[1], MARTIN SAUNDERS[1] & MATT R. KILBURN[1]

[1]*Centre for Microscopy Characterisation and Analysis, and Australian Research Council Centre of Excellence for Core to Crust Fluid Systems, The University of Western Australia, 35 Stirling Highway, Perth, WA 6009, Australia*

[2]*School of Earth Sciences, University of Bristol, Life Sciences Building, 24 Tyndall Avenue, Bristol BS8 1TQ, UK*

[3]*Department of Earth Sciences, University of Oxford, South Parks Road, Oxford OX1 3AN, UK*

[4]*School of Geosciences, University of Aberdeen, Aberdeen AB24 3UE, UK*

[5]*CSIRO Mineral Resources Flagship, Australian Resources Research Centre, Perth, WA 6151, Australia*

[6]*Scottish Universities Environmental Research Centre, East Kilbride, Glasgow G75 0QF, UK*

**Correspondence: David.Wacey@uwa.edu.au*

Abstract: Oxygenation of the Proterozoic atmosphere caused the progressive build-up of dissolved sulphate on the continents and in marine environments. However, oxygen levels in the Proterozoic were low enough to allow the early burial of biological material into low redox potential environments where permineralization and the authigenic replacement of organic material, including micro-organisms, occurred by a range of minerals. Consequently, microbial sulphate reduction caused the widespread degradation of organic matter and, where iron was available, the precipitation of pyrite. By contrast, where sulphate levels were low, early preservation by other minerals (e.g. phosphate or silica) could be excellent. We show, using two Proterozoic lake sequences with low and high sulphate chemistries, but with otherwise similar characteristics, that microbial sulphate reduction caused a profound loss of morphological detail and diversity within preserved microfossils. The results could imply that there is a significant bias in the Proterozoic fossil record towards low sulphate environments, which were in reality relatively scarce.

Many major steps in eukaryote evolution took place during the Proterozoic between *c.* 2000 and 1000 Ma, including the emergence of sexual reproduction and tissue differentiation (Blank 2013; Butterfield 2015). A major problem, however, is posed by the patchy nature of the early fossil record (Cohen & MacDonald 2015). Although remarkably high-quality preservation can be found in some *c.* 1000 Ma freshwater lake deposits (Strother *et al.* 2011; Wacey *et al.* 2014), the marine fossil record of the Proterozoic tends to be rather limited in both quality and diversity. This patchiness is especially surprising in the wider context of taphonomic evolution. Before the Cambrian, which saw the emergence of the metazoan through-gut, sediment bioturbation and silica biomineralization, the redox boundary typically lay much closer to the sediment surface, potentially allowing the rapid encapsulation or permineralization of cellular materials by silicate, pyrite and phosphate (Battison &

†Deceased 16 December 2014.

From: Brasier, A. T., McIlroy, D. & McLoughlin, N. (eds) 2017. *Earth System Evolution and Early Life: A Celebration of the Work of Martin Brasier*. Geological Society, London, Special Publications, **448**, 105–119.
First published online September 15, 2016, https://doi.org/10.1144/SP448.6

Brasier 2012; Wacey *et al.* 2014). However, although acid-resistant vesicles (acritarchs) of inferred eukaryote origin are known from 1.8 Ga and became moderately diverse in nearshore habitats by 1.45 Ga (Lamb *et al.* 2009), overall the mid-Proterozoic record is very limited. Some researchers attribute this to evolutionary stasis in the marine realm during the 'boring billion', when high levels of hydrogen sulphide, which is toxic to eukaryotes, inhibited their evolutionary radiation (Lyons *et al.* 2012), and latterly to the concept that major evolutionary innovations may have mostly been taking place on land at this time (Blank 2013; Wellman & Strother 2015).

The patchy fossil record between *c.* 2000 and 1000 Ma, plus the inability to assign many such fossils to crown groups, markedly influences the extent to which the Proterozoic fossil record may yet be used to calibrate molecular trees (Eme *et al.* 2014). There is a pressing need to identify the controls on fossil preservation and to learn what inferences we might make when the preservation is less good, so that we are not forced to interpret the lack of evidence as biological absence. Preservation depends on a range of factors, including the depositional environment, mineralogy, diagenesis and structural history. In particular, the local fluid chemistry, which, in turn, controls microbial processing and mineral precipitation, may dictate which environments are represented in the fossil record and could bias our interpretations. An excellent opportunity to test this theory is provided by two semi-permanent lake basins preserved within the 1200–1000 Ma Torridonian Supergroup of NW Scotland. Remarkable preservation of organic matter has previously been reported within lake deposits of the *c.* 1000 Ma Torridon Group (specifically the phosphatic horizons and nodules of the Cailleach Head and Diabaig formations; Strother *et al.* 2011; Battison & Brasier 2012; Wacey *et al.* 2014). However, the preservation of organic matter has been reported to be rather poor in mudstones and carbonates of the *c.* 1200 Ma Stoer Group lake deposits (Cloud & Germs 1971) and microfossil recovery using traditional acid maceration approaches has met with only limited success (Strother *et al.* 2011).

In contrast with previous studies that concentrated on fossil material extracted from its host rock, in this work we used petrographic thin sections prepared from laminated calcareous mudstones within the Bay of Stoer Formation of the Stoer Group. We applied a wide range of high spatial resolution morphological and geochemical analytical techniques to characterize newly discovered microfossils and their associated minerals. We then compared and contrasted this style of microfossil preservation with that found in phosphatic deposits of the overlying Torridon Group. This provided a unique opportunity to compare the fossil preservation in Proterozoic lakes with similar amounts of organic matter, similar basement geochemistry and a broadly similar topographic setting (the same Archaean basement surface), but which may have developed different lake chemistries and microbial pathways. We then considered how the preservation of organic matter may be explained in terms of these differing lake biogeochemistries and implications that this may have for the Proterozoic fossil record as a whole.

Geological context

The Torridonian Supergroup consists of two successions separated by a marked angular unconformity (Fig. 1). The lower succession, the Stoer Group, accumulated in fluviatile and lacustrine environments in an extensional basin inboard of the Grenville Orogen on the Laurentian continent (Cawood *et al.* 2007). It has been dated at 1177 $\pm$ 17 Ma (Parnell *et al.* 2011). During the subsequent formation of the Rodinia supercontinent, syn-collisional successions were deposited on the Laurentian craton, including the sandstone-dominated Torridon Group, dated at about 1000 Ma (Diabaig Formation = 994 $\pm$ 48 Ma; Turnbull *et al.* 1996), which is unconformable on the Stoer Group. There is a contrast in the deduced palaeoclimate, which was dry and Mediterranean-like for the Stoer Group and more temperate for the Torridon Group (Stewart 2002). Palaeomagnetic data indicate different locations at latitudes of *c.* 25° N and 30–50° S, respectively (Stewart 2002).

The Torridonian Supergroup includes several horizons interpreted to include lacustrine environments from which diverse assemblages of microfossils have been obtained (Cloud & Germs 1971; Strother *et al.* 2011; Battison & Brasier 2012). Their lacustrine context is suggested by packaging within red fluvial sediments, the predominance of small ripple sets, mud cracks and rain pits (Stewart 2002), the presence of varve-like lamination (Andrews *et al.* 2010) and by the absence of large ripples or tidal features. The Stoer Group sediments are notably evaporitic with carbonate, sulphate and pyritic deposits, including those within the black shale lake sediments of the Poll a Mhuilt Member of the Bay of Stoer Formation (Parnell *et al.* 2010). The determination of annual lamination in the black shale is strong evidence for seasonal lacustrine deposition. By contrast, the Torridon Group deposits are typically non-evaporitic and sulphate-poor and include the lacustrine deposits of the Cailleach Head and Diabaig formations (Fig. 1). These distinctions are evident from the high sulphur content and sulphur to organic carbon ratios (mean

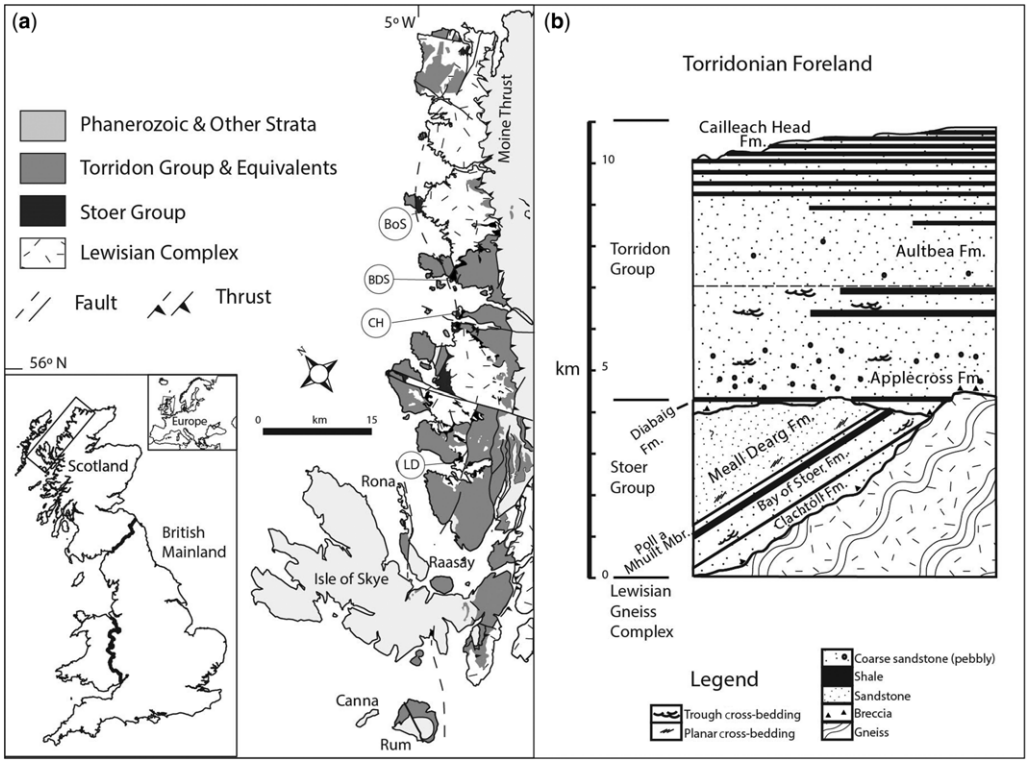

Fig. 1. Stratigraphy of the Torridonian Supergroup and map of NW Scotland showing sampling levels and localities. Samples collected from the Stoer Group, Bay of Stoer (BoS), the Diabaig Formation, Badenscallie (BDS) and Lower Diabaig (LD), and the Cailleach Head Formation at Cailleach Head (CH).

S : C = 3.56, $n = 85$) of the Bay of Stoer Formation, Stoer Group and the uniformly low S to C ratios (mean S : C = 0.35, $n = 104$) of the Cailleach Head and Diabaig formations of the Torridon Group (Fig. 2), even though the carbon contents of the two formations are otherwise similar (0–0.5%, mean *c.* 0.2% total organic carbon; Spinks *et al.* 2014). The high and low S to C ratios are reflected in the abundance and paucity of pyrite, respectively. Both sequences have experienced low-grade metamorphism (Stewart 2002), but both show comparable very good preservation of sedimentation features and primary variations in geochemistry. The contrasts between the two groups are summarized in Table 1. This paper combines hitherto independent studies of sulphate chemistry and microfossil preservation to show how they are related.

Methods

Determination of sulphur to carbon ratios

The sulphur and organic carbon contents were measured to a precision of $\pm 0.5\%$ using a LECO CS225 elemental analyser after decarbonization with hydrochloric acid.

Sulphur isotope analysis

The sulphur isotope composition of both the sulphide and sulphate components was measured in a whole rock sample of Bay of Stoer Formation shale using the chromium reduction method of Canfield *et al.* (1986). The H_2S generated from the reduction of sulphide sulphur by $CrCl_2$ was trapped as Ag_2S in a solution of $AgNO_3$. The resulting sulphide was washed, dried and analysed by conventional procedures following the method of Robinson & Kusakabe (1975). All the sulphur isotope data are reported in $\delta^{34}S$ notation as per mil (‰) variations from the Vienna Canyon Diablo Troilite (V-CDT) standard.

The sulphur isotope compositions of pyritized microfossils from the Bay of Stoer Formation were determined using a CAMECA IMS 1280 ion microprobe operating in the multi-collection mode at Centre for Microscopy Characterisation and Analysis (CMCA), University of Western Australia.

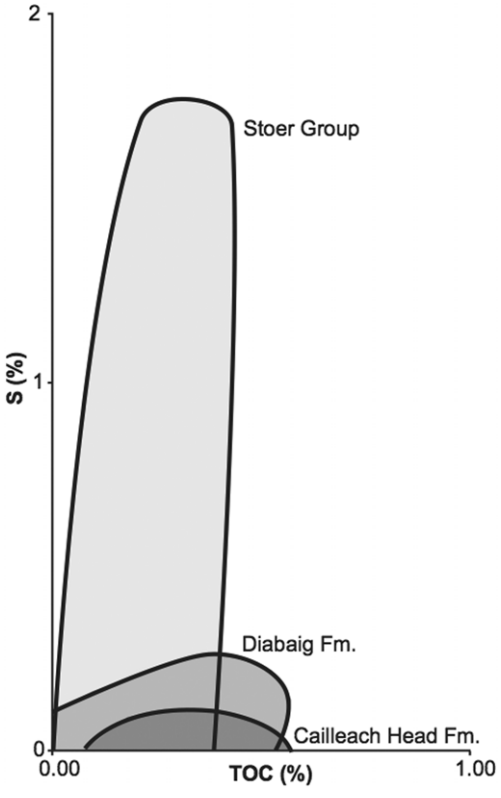

Fig. 2. Cross-plot of total organic carbon (TOC) (%) and S (%) contents in Torridon Supergroup shales showing data fields for the Stoer Group, Diabaig Formation and Cailleach Head Formation. Only the Stoer Group is characterized by high sulphur to carbon ratios (mean 3.56, $n = 85$), an order of magnitude greater than in the Diabaig Formation (mean 0.35, $n = 92$) and the Cailleach Head Formation (mean 0.34, $n = 12$).

The analytical protocol used the rastered beam approach outlined in Farquhar *et al.* (2013). The external precisions of $^{34}S/^{32}S$ on the SON-3 (pyrite) standard for the two analytical sessions were 0.2‰ (2 SD; $n = 14$) and 0.1‰ (2 SD; $n = 10$). The sample count rates varied between *c.* 5 and 90% of the count rate of the standard; however, there was no observed correlation between the secondary count rate and the $\delta^{34}S$ value of the samples. Instrumental mass fractionation and the propagation of uncertainty also followed the protocol in Farquhar *et al.* (2013). The uncertainty terms included the internal uncertainty, the external uncertainty of the instrumental mass fractionation of the primary standard and the uncertainty of the standard relative to V-CDT.

Table 1. *Comparison of Stoer Group and Torridon Group lacustrine units*

	Stoer Group (1177 Ma)	Torridon Group (*c.* 1000 Ma)
Total organic carbon (mean wt%)	0.22	0.19
Shale sulphur to carbon ratio	3.56	0.35
Shale burial rate (mm a^{-1})	0.36	0.38
Evaporites	Gypsum	None
Pyrite residence	Shale	Sandstone
Fossil preservation	Poor	Good
Carbon identifiable as bioelements (%)	<1	>20
Mineral growth on fossils	Silica, carbonate, pyrite	Phosphate, clay

Focused ion beam milling combined with scanning electron microscopy

Focused ion beam milling combined with scanning electron microscopy was performed on a Zeiss Neon 40 dual-beam instrument at the Electron Microscopy Unit, University of New South Wales. The protocol followed that reported by Wacey *et al.* (2012), with the final milling and image capture parameters adjusted to suit the type of sample being analysed. For both the Bay of Stoer Formation and comparative Cailleach Head Formation material, the milling depth was *c.* 20 μm using a 2 nA ion beam current and the electron beam images were acquired with a *c.* 30 s capture time at 5 kV.

Transmission electron microscopy

Transmission electron microscopy (TEM) data were obtained from focused ion beam milled wafers using a JEOL 2100 LaB_6 transmission electron microscope equipped with a Gatan Orius charge-coupled device camera and a Tridiem energy filter, together with an FEI Titan G2 80–200 TEM/STEM with ChemiSTEM technology. Both instruments are located in the CMCA and were operated at 200 kV. Energy-filtered TEM elemental maps on the JEOL 2100 instrument were obtained using the conventional three-window technique (Brydson 2001) with the energy windows selected to provide the optimum signal-to-noise ratios.

Nanoscale secondary ion mass spectrometry

Ion mapping of the Bay of Stoer Formation microfossils was performed using a CAMECA

NanoSIMS 50 instrument at CMCA, with the instrument parameters optimized as described in Wacey *et al.* (2011). The analysis areas were 30 × 30 μm at a resolution of 256 × 256 pixels and 45 × 45 μm at a resolution of 512 × 512 pixels (each pixel measuring 117 nm in the former and 88 nm in the latter), with a dwell time of 45 ms per pixel, and a primary beam current of *c.* 2.5 pA. The secondary ions mapped were $^{16}O^-$, $^{24}C_2^-$, $^{12}C^{14}N^-$, $^{34}S^-$ and $^{56}Fe^{32}S^-$, and charge compensation was achieved using an electron flood gun.

Laser Raman microspectrometry

Laser Raman analyses were carried out at the University of Bergen using a Horiba LabRAM HR800 integrated confocal Raman system and LabSpec5 acquisition and analysis software. Samples were standard uncovered geological thin sections, allowing the optical and chemical maps to be superimposed. All analyses were carried out using a 514.5 nm laser, 100 μm confocal hole, 1800 grating and ×50 objective lens. The laser was focused at least 1 μm below the surface of the thin sections to avoid surface polishing effects. Dual acquisitions were taken from each analysis point, each with an acquisition time of 4 s, to identify the minerals from the Raman spectra. Raman maps were acquired with a 1.5 μm spatial resolution.

Results

Fossil preservation in the Stoer Group

Thin sections from the Bay of Stoer Formation of the Stoer Group invariably yield rather poorly preserved microfossils. Under the optical microscope microfossils appear to be confined to sparse remains, many of which have an uneven, dappled surface texture and walls that appear broken or missing in places (Fig. 3). The microfossil morphotype diversity is rather low, ranging from roughly spherical to more elongate and collapsed bag-like forms, with rare examples containing smaller interior coccoid structures (Fig. 3). The microfossils are comparatively large, commonly 20–100 μm in diameter, and are restricted to parts of the thin sections that are rich in an opaque mineral, identified (using reflected light, Raman and nanoscale secondary ion mass spectrometry (NanoSIMS); Fig. 4) as pyrite. The three-dimensional preservation of most organisms (Figs 3 & 4) attests to early fossilization prior to compaction.

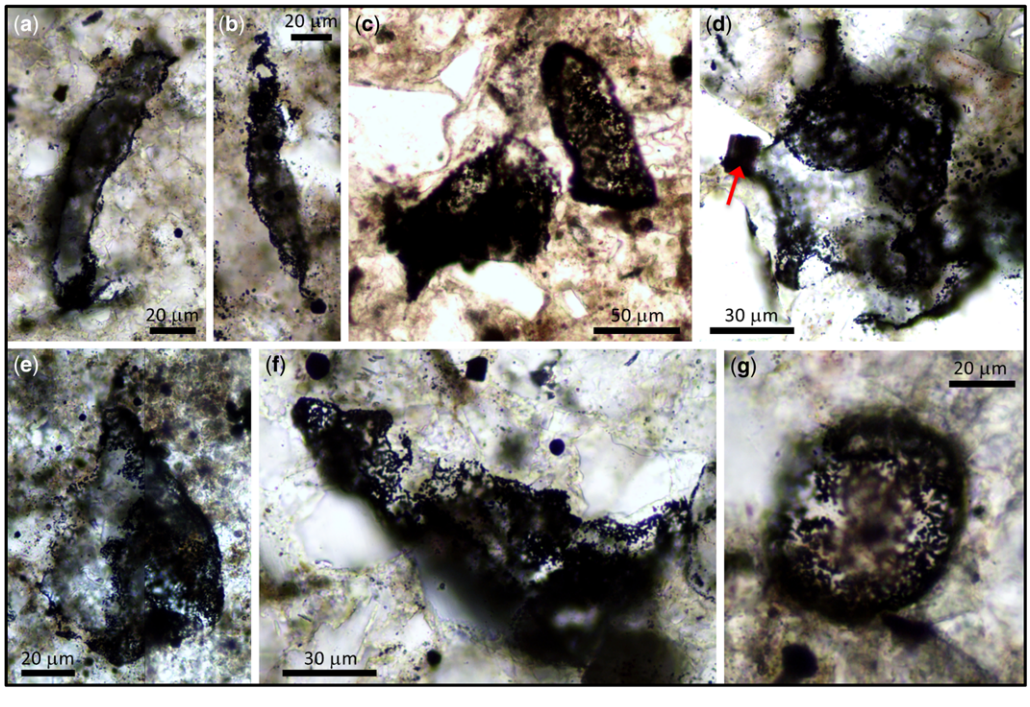

Fig. 3. Examples of moderate to poor quality microfossil preservation in pyrite from the Bay of Stoer Formation, including (**a**, **b**) filaments, (**c**, **e**, **f**) bag-like vesicles, (**d**) vesicles with putative internal spheroids and (**g**) spheroids. Arrow in (d) indicates the position of wafer extracted for transmission electron microscopy (data shown in Fig. 5).

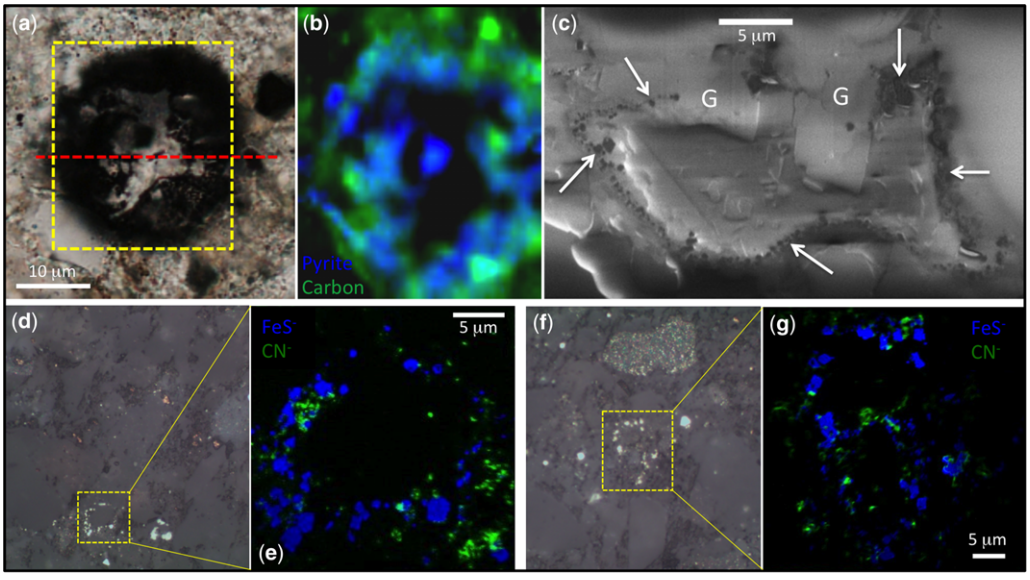

Fig. 4. Characterization of the style of microfossil preservation within the Bay of Stoer Formation. (**a**) Transmitted light photomicrograph of a pyritized vesicle. (**b**) Laser Raman map of the boxed area in part a. Pyrite (mapped using the *c.* 380 cm^{-1} Raman band) is shown in blue and organic carbon (mapped using the *c.* 1600 cm^{-1} Raman band) is shown in green. (**c**) Scanning electron microscopy image of a focused ion beam milled cross-section through the vesicle shown in part a (milled face marked by dashed red line in part a), showing multiple small pyrite grains aligned in narrow zones along the former vesicle wall (e.g. arrows). Note that the gaps (G) in the upper part of the vesicle wall correspond to the non-pyritized area in the optical image. **(d–g)** Reflected light images (parts d and f) and accompanying nanoscale secondary ion mass spectrometry (NanoSIMS) ion maps (parts e and g) of two further microfossils from the Bay of Stoer Formation. Yellow boxes indicate the areas analysed by NanoSIMS. In the NanoSIMS ion maps, pyrite (analysed as FeS^-) is shown in blue, with organic material (analysed as CN^-) shown in green. The pyrite and organic material are intimately related, but there is no continuous organic structure that would indicate pristine, non-decomposed cell or vesicle walls.

Pyrite occurs in distinct narrow zones and, in most of the microfossil specimens analysed, it is intimately associated with organic carbon, with both phases outlining the shape of the microfossil walls (Fig. 4b, e, g). Organic carbon and pyrite are rarely present in the interior of the microfossils, consistent with optical images suggesting little or no preservation of cellular contents in these samples. There is a gradation in the amount of organic carbon retained within the microfossil walls (compare Figs 4 & 5) and, in rare examples, all the organic carbon has been replaced (Fig. 5). In these instances the microfossil walls are instead denoted by narrow zones of closely spaced micro-pyrite grains plus aluminosilicates (Fig. 5). Two types of aluminosilicate occur within and adjacent to the microfossil walls: the more abundant phase is magnesium- and iron-rich and the minor phase is potassium-rich. These have a flaky habit and both their habit and distribution are similar to the clay minerals described in a study of microfossils from the overlying Torridon Group (Wacey *et al.* 2014). Other mineral phases occurring either in the microfossil interior or nearby in the sediment matrix include calcite, anatase, quartz and feldspar, broadly consistent with the known calcitic mudstone lithology in which the microfossils are found. Where the preservation is poor, all the organic matter lacks detail, rather than a patchy preservation that could be attributed to partial replacement by a mineral such as calcite, or corrosion by an aggressive fluid.

Sulphur isotope compositions

In addition to the existing database for sulphide separates from the Stoer Group, which shows values lighter than −30‰ and a high degree of fractionation from coeval sulphates (Parnell *et al.* 2010), a new whole rock analysis from the Bay of Stoer Formation yielded measurements for sulphide and sulphate components of −31.7 and −35.3‰, respectively. Ion microprobe data from macroscopic pyrite within a Bay of Stoer rock chip gave $\delta^{34}S$ values between −34.2 and −38.7‰ with a mean of −35.5‰ ($n = 16$; Table 2; Fig. 6). This mean value closely replicated the previously reported

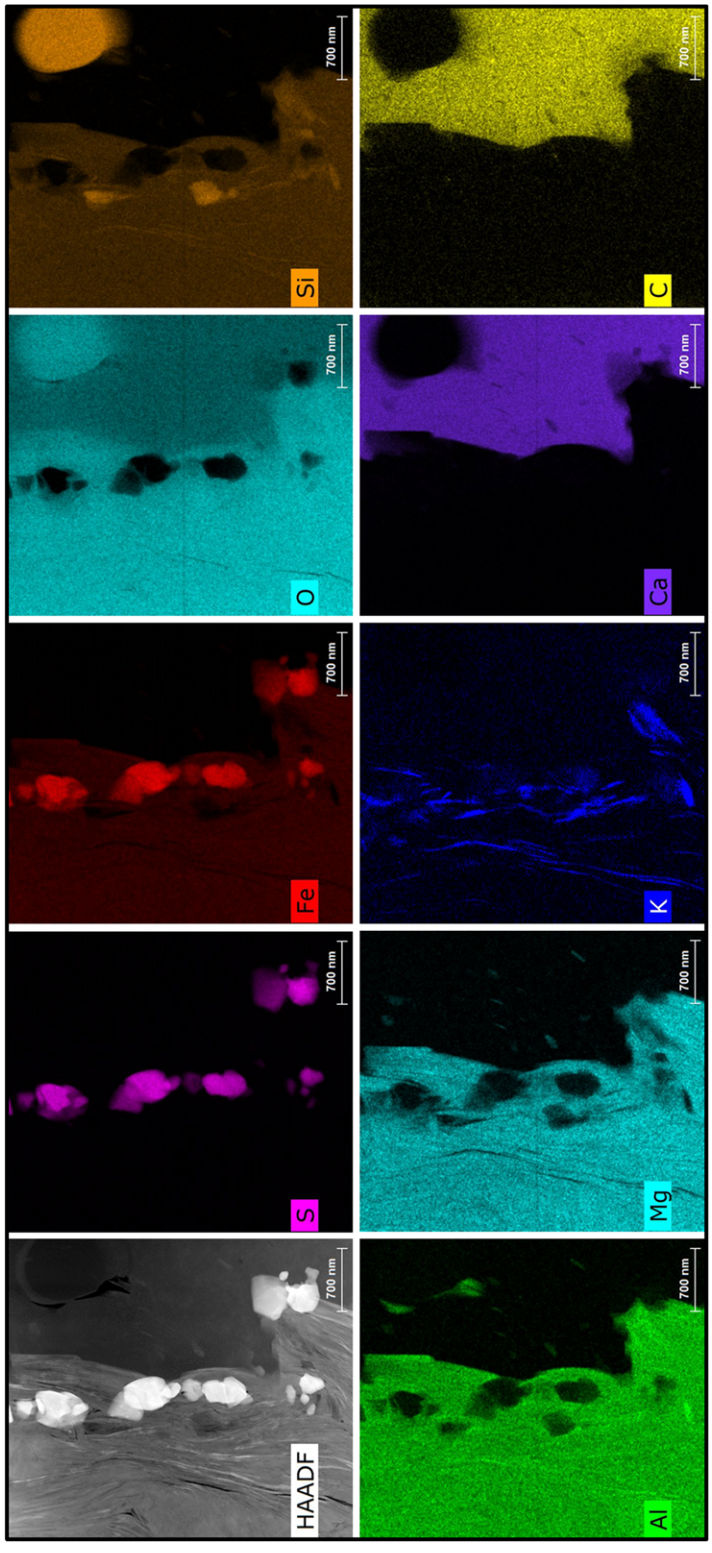

Fig. 5. Nanoscale analysis of a pyritized microfossil wall using transmission electron microscopy. High-angle annular dark field (HAADF) image plus elemental maps of a pyritized microfossil wall (from the microfossil shown in Fig. 3d). The brightest correlated regions in the iron and sulphur maps indicate pyrite, whereas those in the calcium and carbon maps indicate calcite. Aluminosilicates are indicated by correlations in aluminium, oxygen, silicon and either iron, magnesium or potassium. Quartz is indicated by the correlation of silicon and oxygen, but the anti-correlation of aluminium and other elements. These data show that the organic material of the microfossil wall has been completely replaced by pyrite and aluminosilicates. Two types of aluminosilicate are present: a minor potassium-rich variety occurring very close to the pyrite and possibly replicating the original microfossil wall; and a major Mg- and Fe-rich variety that replicates the fossil wall and extends exterior to the former wall. Calcite is found interior to the former wall, whereas minor quartz is found both within and interior to the wall zone.

Table 2. *In situ sulphur isotope data obtained using a CAMECA IMS 1280 instrument*

Analysis ID	^{34}S counts	$\delta^{34}S_{V-CDT}$	$\pm 2\sigma$ (‰)
Standards			
Session 1	($\times 10^7$)		
SON-3_1	8.06	1.5	0.3
SON-3_2	8.22	1.5	0.3
SON-3_3	8.42	1.6	0.3
SON-3_4	8.43	1.6	0.3
SON-3_5	8.57	1.6	0.3
SON-3_6	8.44	1.7	0.3
SON-3_7	8.36	1.9	0.3
SON-3_8	8.39	1.7	0.3
SON-3_9	7.99	1.6	0.3
SON-3_10	7.94	1.7	0.3
SON-3_11	7.86	1.6	0.3
SON-3_12	7.90	1.6	0.3
SON-3_13	7.71	1.7	0.3
SON-3_14	7.81	1.7	0.3
		Mean = 1.6	
		$2\sigma = 0.2$	
Session 2	($\times 10^7$)		
SON-3_1	10.6	1.6	0.2
SON-3_2	10.5	1.6	0.2
SON-3_3	10.3	1.6	0.2
SON-3_4	10.1	1.5	0.2
SON-3_5	9.94	1.7	0.2
SON-3_6	9.94	1.7	0.2
SON-3_7	9.72	1.7	0.2
SON-3_8	9.61	1.6	0.2
SON-3_9	9.54	1.6	0.2
SON-3_10	9.47	1.6	0.2
		Mean = 1.6	
		$2\sigma = 0.1$	
Macroscopic pyrite			
JPT_1	6.90	−36.2	0.3
JPT_2	7.18	−38.7	0.3
JPT_3	7.00	−37.2	0.3
JPT_4	7.43	−35.2	0.3
JPT_5	6.90	−35.8	0.3
JPT_6	7.31	−34.7	0.3
JPT_8	6.91	−34.5	0.3
JPT_9	6.98	−35.2	0.3
JPT_10	7.19	−34.3	0.3
JPT_11	6.93	−35.2	0.3
JPT_12	6.83	−36.6	0.3
JPT_13	7.01	−34.5	0.3
JPT_14	6.81	−35.7	0.3
JPT_15	6.71	−34.2	0.3
JPT_18	6.59	−35.7	0.3
JPT_20	6.77	−34.6	0.3
Microscopic pyrite			
PAR_1	3.48	−48.7	0.3
PAR_2	0.42	−45.8	0.3
PAR_3	1.32	−47.1	0.3
PAR_4	2.19	−48.0	0.3
PAR_5	1.94	−46.7	0.3
PAR_6	0.44	−48.8	0.3
PAR_7	0.93	−48.4	0.3
PAR_8	1.65	−47.5	0.3

Data from sample JPTOR19 were collected adjacent to those previously obtained using laser ablation gas source mass spectrometry (Parnell *et al.* 2010; see Fig. 6 for precise location of analysis spots). Data from sample PAR401 were collected from individual pyritized microfossils (see Fig. 7 for precise location of analysis spots).

laser ablation value (mean −35.4‰; Parnell *et al.* 2010), showing that the ion microprobe data are both accurate and reproducible. Ion microprobe analyses of the sulphur isotope compositions of pyritized microfossils in the Bay of Stoer Formation gave very light and consistent $\delta^{34}S$ values (−45.8 to −48.8‰; $n = 8$; Table 2; Fig. 7). No sulphur isotope data were collected from the Cailleach Head or Diabaig formations because these samples are pyrite-poor and pyrite has not been observed replacing microfossil organic material.

Fossil preservation in the Torridon Group

The Torridon Group shows a gradation in the fidelity of preservation of microfossils, as expected for any large population of organisms, some of which would have been alive and others at various stages of decomposition when fossilized. However, the Torridon Group is particularly notable for very high fidelity preservation within the phosphatic horizons and nodules of the Cailleach Head and Diabaig formations (Strother *et al.* 2011; Battison & Brasier 2012; Wacey *et al.* 2014). Here, microfossil preservation is among the highest quality known in the entire Precambrian rock record, with light-coloured kerogen outlining not only intact microbial sheaths and multi-laminated or sculptured vesicles, but also clusters of cells, some with their contents partly intact (Fig. 8). Excellent three-dimensional preservation is facilitated by the encapsulation of organic material within francolite (calcium fluorapatite) and clay minerals (Fig. 9; see also Wacey *et al.* 2014). We found that the proportion of organic matter identifiable in thin sections as cells, sheaths or vesicles was typically >20%. In contrast with the Stoer Group, cellular and subcellular features are composed entirely of kerogenous organic carbon (Fig. 9b–f); mineral phases such as clays and phosphate appear to have nucleated on this material, but not grown within it or replaced it (Fig. 9c, f). Neither the encapsulation nor replacement of cellular

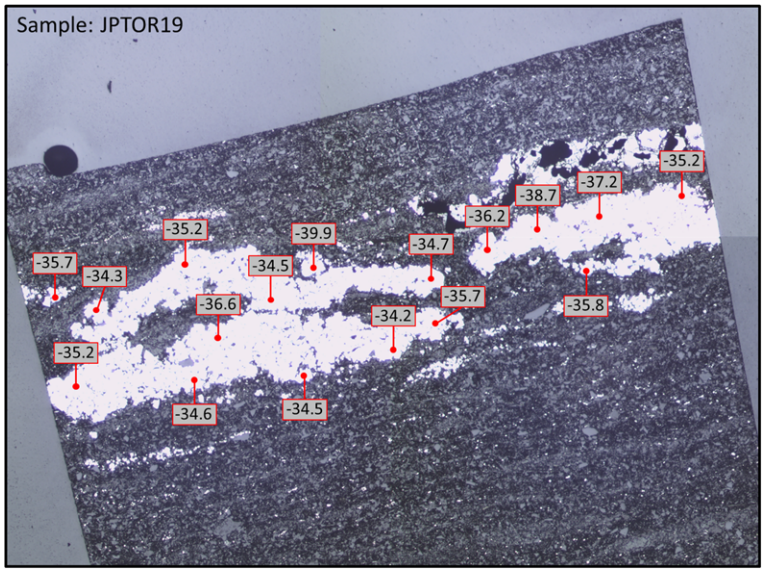

Fig. 6. Spatially resolved sulphur isotope data ($\delta^{34}S‰$ V-CDT) from macroscopic pyrite within the Bay of Stoer Formation sample JPTOR19. The mean of these data points (−35.5‰) closely replicates the 'bulk' value of these pyrite nodules obtained previously using laser ablation gas source mass spectrometry (−35.4‰; Parnell *et al.* 2010).

organic material by pyrite was observed in the phosphate nodules and horizons of the Torridon Group.

We therefore found a clear distinction in the fidelity of microfossil preservation between the phosphatic sediments of the Torridon Group, characterized by kerogenous cellular material preserving exquisite morphological detail and lacking pyritization, and the Stoer Group, possessing microfossils with degraded and partially replaced organic matter with a conspicuous degree of pyritization (compare Figs 4 & 5 with Fig. 9). This raises the possibility that these contrasts were related, at least in part, to the absence or presence of well-developed sulphur metabolic pathways in the contrasting lake ecosystems.

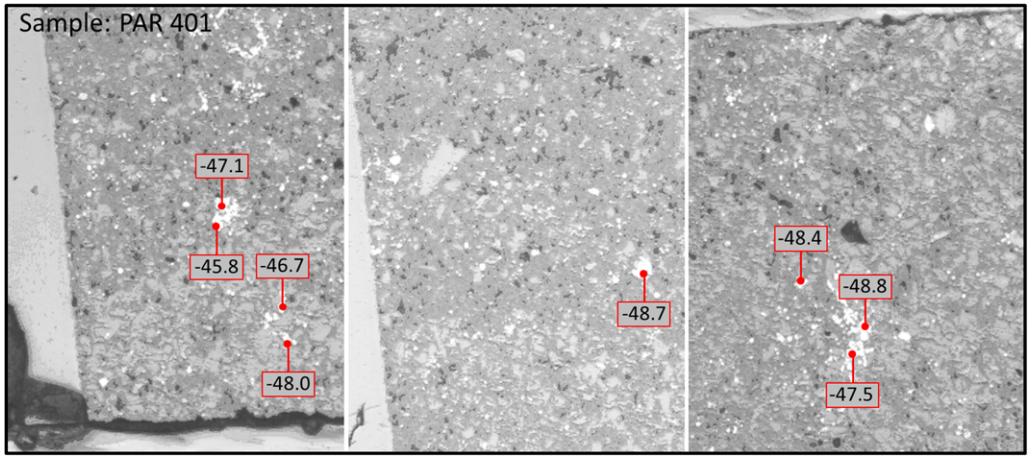

Fig. 7. Spatially resolved sulphur isotope data ($\delta^{34}S‰$ V-CDT) from pyritized microfossils within the Bay of Stoer Formation sample PAR401.

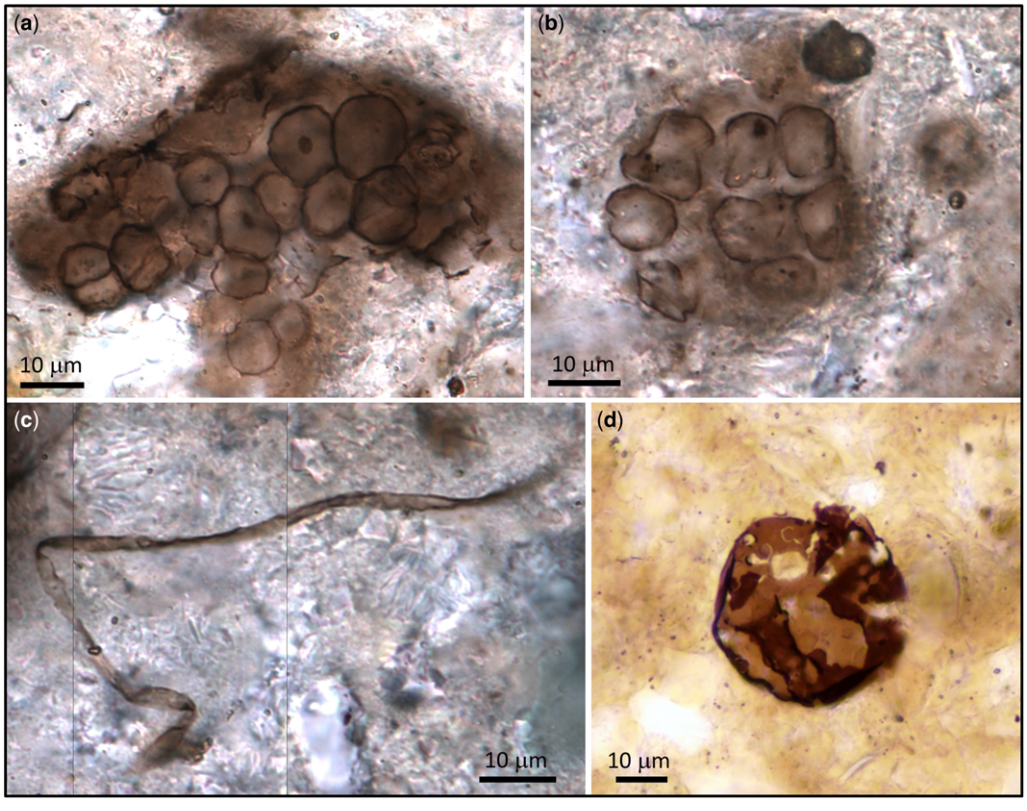

Fig. 8. Examples of high-quality microfossil preservation in phosphate and phyllosilicate from the Torridon Group, including (**a**, **b**) clusters of coccoids with partially preserved cell contents, (**c**) twisted filaments and (d) larger spheroidal vesicles. Note the holey appearance of the vesicle in (d), here attributed to heterotrophic microbial decay.

Discussion

Fossil preservation

Pyritization is one of the processes that commonly causes the authigenic mineralization of organic matter, particularly in fine-grained organic-rich sediments, where dissolved iron reacts with the hydrogen sulphide produced by microbial sulphate reduction (MSR). A microbial origin for sulphate reduction can typically be evidenced from a large degree of sulphur isotope fractionation, as reported previously in the Stoer Group (Parnell *et al.* 2010) and reinforced by our new data. The precipitation of pyrite is controlled by the availability of metabolizable organic matter, plus the availability of sulphate and ferrous iron, with a balance between the decay of organic matter and its preservation by mineralization (Briggs *et al.* 1996; Schiffbauer *et al.* 2014). Pyrite formation rarely occurs early enough to preserve soft tissues (Briggs *et al.* 1991). In most instances, the organic matter associated with pyrite in the rock record is conspicuously degraded, which requires a timescale of only months to achieve (Sagemann *et al.* 1999).

The pyritization process provides a logical explanation for the contrasts in preservation between microfossils seen in the Stoer and Torridon groups. If iron and sulphate are plentiful in the early stages of heterotrophic activity, then labile organic matter will be fully consumed to precipitate pyrite. Hence the intracellular contents, delicate cells and trichomes will be the first organic structures to be degraded by sulphate-reducing microbes and there will be no trace of these as fossils, with pyrite precipitation typically occurring as framboids and micro-grains (which are plentiful in the Bay of Stoer thin sections). Later, the more resistant sheaths and vesicles will start to be consumed; we infer that iron was less plentiful by this stage (sulphate may also start to be depleted, but our $\delta^{34}S$ data suggest this was not the case here) and the precipitation of pyrite was proximal on and within the vesicle walls.

The high rates of sedimentation in lakes compared with oceans means that organic matter in

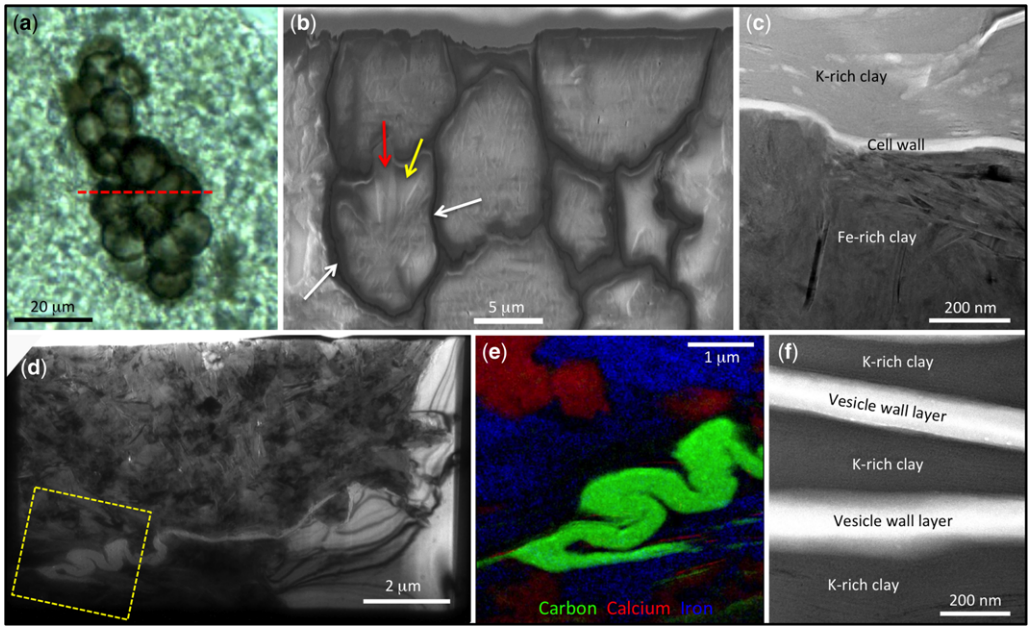

Fig. 9. Characterization of the style of microfossil preservation in the Torridon Group (cf. Figs 4 & 5 from the Stoer Group) (**a**) Transmitted light photomicrograph of a cluster of carbonaceous cells, Cailleach Head Formation, Torridon Group. (**b**) SEM image of focused ion beam milled cross-section through the cells shown in part a (milled face marked by dashed red line in part a), showing dark, narrow, continuous carbonaceous cell walls (white arrows) preserved by apatite (red arrow) and fine-grained clay minerals (yellow arrow). (**c**) Bright-field transmission electron microscopy (TEM) image showing an intact carbonaceous cell wall encapsulated by potassium-rich and iron-rich clay minerals from the Diabaig Formation. (**d**) Bright-field TEM image of about one-quarter of a cell from the Cailleach Head Formation showing thick, folded cell wall (best seen in boxed area). (**e**) Elemental maps from the boxed area in part d showing carbonaceous cell wall (green) preserved in apatite (represented by calcium, red) and iron silicate (blue). (**f**) Bright-field TEM image of a vesicle from the Diabaig Formation exhibiting a multi-layered wall exquisitely preserved in potassium-rich clay minerals. Adapted from Wacey *et al.* (2014).

lakes may be more rapidly and efficiently conveyed down into the anaerobic zone (Spinks *et al.* 2014). Both experiments (Sagemann *et al.* 1999) and fossil studies (Wacey *et al.* 2013) reveal that MSR can result in the conspicuous heterotrophic remineralization of organic matter, resulting in the degradation of organisms and, under favourable iron-rich conditions, pyritization. There is a strong interrelationship between organic matter and MSR. The rate of MSR (if iron and sulphate are non-limiting) is controlled by the availability of organic matter and MSR causes the breakdown of the organic matter (Westrich & Berner 1984). The degree of breakdown depends on the type of organic matter, but freshly deposited micro-organisms are susceptible to rapid decomposition (Westrich & Berner 1984). As sulphate reduction is a more efficient source of energy than other anaerobic pathways, such as fermentation and methanogenesis, it can process organic material at a faster rate and to a greater degree. Studies in some modern lakes show that 80–90% of the total organic matter is decomposed by sulphate reduction during the summer when the lakes become stratified (Krevs & Kucinskiene 2012). The Bay of Stoer Formation black shales are the deposits of a stratified lake (Andrews *et al.* 2010), so may have similarly experienced significant MSR.

Heterotrophic activity in the absence of sulphate would still result in some degradation of organic material, as evidenced by the holes in some Torridon Group cells and vesicles (Fig. 8d), but this would not be driven by sulphate-reducing bacteria and pyrite would not precipitate. Fermentation and methanogenesis degradation pathways are significantly less efficient at processing organic material. This, combined with early encapsulation of cellular material by clay minerals and phosphate, would have limited the loss of morphological detail in the Torridon Group microfossils. An absence of iron may also result in a lack of pyrite precipitation even if sulphate is plentiful. However, the presence of syngenetic iron-rich clay minerals encapsulating the Torridon Group microfossils (Fig. 9c, e; see also

Wacey *et al.* 2014) strongly suggests that it was sulphate, not iron, which was the missing ingredient preventing the formation of pyrite in the Torridon Group lakes. This is consistent with heavy sulphur isotope values in the Torridon Group (Parnell *et al.* 2010), which suggest a limited sulphate reservoir.

The rates of deposition of the Stoer and Torridon lake sediments were similar and fairly rapid (Spinks *et al.* 2014). Diagenetic mineral growth around microfossils was also rapid, leading to three-dimensional preservation, and was carbonate, silicate and pyrite in the Stoer lakes (Figs 4 & 5) and phosphate and phyllosilicate in the Torridon lakes (Fig. 9; see also Strother *et al.* 2011; Wacey *et al.* 2014). If the composition of the organic matter was also similar, and there is no reason to assume otherwise, the more altered (including pyritic) state of preservation of the organic matter in the Stoer lakes may be explained by higher rates of sulphate reduction as a result of the freely available sulphate in the lake waters. Conversely, the less altered organic matter in the Torridon lake ecosystems seems to have been related to the lack of extensive sulphate reduction on or beneath the lake floor. This allowed much slower rates of organic matter degradation with the encapsulation of almost pristine organic material and the retention of exquisite anatomical detail.

Sulphur isotope compositions

The inference of MSR in the Bay of Stoer Formation is strongly supported by very light sulphur isotope compositions. The sulphur isotope data from sulphide nodules in the Bay of Stoer shales show a marked fractionation (up to 55‰) relative to contemporary sulphate sampled in red beds and are interpreted to reflect MSR in the lacustrine sediments (Parnell *et al.* 2010). The new data, from the separated sulphate and sulphide fractions of a whole rock shale sample, show that both fractions are characterized by light isotopic compositions (lighter than −30‰). Petrographic data show that the sulphate post-dated the sulphide (Parnell *et al.* 2014). This implies that the sulphate fraction in the shale was oxidized from the microbially reduced sulphide. Sulphide oxidation can also be microbially mediated, with negligible isotopic fractionation (Brabec *et al.* 2012), consistent with the measured Stoer Group $\delta^{34}S$ data.

Pyrite precipitated on and around decaying micro-organisms records very light and rather consistent $\delta^{34}S$ values, even lighter than the values reported from the early diagenetic pyrite nodules and the whole rock data. This may indicate the control of MSR by a different population of bacteria and/or the increased cycling of sulphur in these microenvironments. However, this very light pyrite represents a very limited proportion of the total pyrite and therefore does not affect the bulk isotopic composition.

Implications for the fossil record

The data from the Torridonian Supergroup indicate that the high-fidelity morphological preservation of microscopic organic cellular material is favoured in environments conducive to phosphatization and clay mineral precipitation, as opposed to pyritization. Given that the presence of sulphate, rather than iron, appears to determine whether pyritization occurs in these lakes, this raises the intriguing possibility that sulphate-poor environments may have better preserved fossil records than sulphate-enriched environments. Could this mean that Proterozoic shallow marine and terrestrial environments, where much of the fossil record of this age is found, have records that are biased by the pathways of decomposition?

There was an increased probability of sulphate-rich conditions in shallow marine and terrestrial environments after the Great Oxidation Event, at least by the latter part of the Mesoproterozoic (Kah *et al.* 2004). Evidence for sulphate evaporites in the Mesoproterozoic is emerging on several palaeocontinents (Parnell *et al.* 2015). There are a number of examples in shallow water/terrestrial Proterozoic fossil assemblages where microfossils show a lower fidelity of preservation when pyritized than the adjacent non-pyritized specimens. These include the 1878 Ma Gunflint Formation, where organic microfossils encapsulated and permineralized in silica retain additional morphological features to those only a few micrometres away that have been pyritized (Wacey *et al.* 2013). In the *c.* 1650 Ma Amelia Dolomite from the Northern Territory of Australia, pseudomorphs of gypsum (calcium sulphate, a source of sulphate for MSR) occur in close proximity to abundant microfossils (Muir 1976). Furthermore, cells assigned to *Sphaerophycus reticulatum* that occur with abundant pyrite have been noted as being particularly decomposed compared with other genera in the same silicified horizon (Muir 1976, fig. 6) and examples of pyrite growing along the outlines of cell walls at advanced stages of decomposition have also been reported (Muir 1976, fig. 7).

In the *c.* 1450 Ma Wumishan Formation of northern China, gypsum crystals co-occur with pyrite crystals and very poorly preserved microfossils in thrombolites, although the quality of microfossil preservation may also have been adversely affected by carbonate precipitation in this setting (Tang *et al.* 2013). In the *c.* 1200 Ma Angmaat Formation of Baffin Island, gypsum is again commonly

associated with the chert nodules that preserve microfossils (Knoll *et al.* 2013). Here, silicified microfossils show high-fidelity preservation (e.g. Knoll *et al.* 2013, figs 3 and 4), but microfossils are rare (and poorly preserved) to absent in zones where the organic material experienced early diagenetic pyritization. In the 750 Ma Chuar Group from the Grand Canyon, vase-shaped microfossils preserved as casts coated with pyrite provide less wall definition that those preserved as siliceous or organic-coated casts (Porter & Knoll 2000). By contrast, in mid-Proterozoic sediments where preservation is particularly good, pyrite is conspicuously lacking – for example, in the Changchang Group, north China (Lamb *et al.* 2009). These relationships are consistent with those observed in the Torridonian Supergroup and the combined evidence suggests that the heterotrophic consumption of cellular organic material by sulphate-reducing bacteria may have restricted the quality of the Proterozoic fossil record. The age range over which these contrasts are observed implies that the *c.* 200 myr age difference between the two deposits in the Torridonian Supergroup is not a critical factor. The examples where pyritized and non-pyritized fossils occur in close proximity serve to emphasize the relevance of pyritization to preservation. However, the more general examples are of either good (non-pyritized) or poor (pyritized) preservation. This potentially leads to bias, where the best-preserved fossils are from environments with anomalously low sulphate contents or very early permineralization by other anomalous pore water chemistries.

The norm, which in Mesoproterozoic marine rocks may be sulphate concentrations of a few mM (Kah *et al.* 2004), may not engender good preservation. The Torridonian example of a sulphate-rich deposit is lacustrine, although the majority of the surviving Mesoproterozoic record is marine. However, the relevance of sulphate-rich pore waters to fossil preservation is independent of environment. Any perception that lake deposits are predominantly freshwater may also be erroneously biased by the current environment because the geological record shows that periods of widespread continental sedimentation commonly contain sulphate-rich terrestrial deposits (Warren 2010).

There would have been more rapid changes in redox conditions near the surface during the early stages of burial in the Proterozoic, with the precipitation of organic-stabilizing minerals more likely than during the Phanerozoic. Lower levels of atmospheric oxygen meant less penetration of oxygen into the surface sediments. There was a lack of bioturbation and scavenging in marine environments before the Cambrian (Canfield & Farquhar 2009). Changes in the redox potential therefore took place at shallower sediment depths than in the Phanerozoic. In lakes, in particular, because of their greater mean sedimentation rate (Spinks *et al.* 2014), sediments rapidly passed through the zone of near-surface oxidation and into a realm where MSR and the precipitation of pyrite, phosphate and other minerals occurred. The contrasting history between sulphate-rich and sulphate-poor environments was therefore especially pronounced in these Proterozoic continental successions. The sulphate level in the Phanerozoic ocean was higher than in the Proterozoic, but this should not be a critical factor. Sulphate levels were already sufficiently high in the Mesoproterozoic ocean to cause massive gypsum precipitation and the presence of sulphate-saturated pore waters. With such a high availability of sulphate, the control on the degree of sulphate reduction to form pyrite is more likely to be the availability of organic matter or iron.

We interpret the Stoer lakes to have formed under conditions of interior, closed drainage under a warm, semi-arid climate conducive to evaporation and the formation of calcium carbonate and calcium sulphate. Abundant sulphate ions allowed for a fully expressed range of sulphur isotope fractionation during bacterial sulphate reduction and may also have led to episodically euxinic conditions in the deeper lake. By contrast, the younger Diabaig and Cailleach Head lakes formed under conditions with open rather than enclosed drainage and the climate was conceivably more temperate. Neither carbonate nor sulphate grew as authigenic precipitates on the lake floor. Instead, phosphate ions were concentrated during the degradation of organic matter and calcium phosphate readily precipitated when the redox conditions were favourable.

Conclusion

An important development during the Mesoproterozoic was the expansion of environments with sulphate evaporites as a consequence of the oxidative weathering of sulphide minerals in continental rocks. These environments were fundamental habitats for sulphate-reducing bacteria, which could utilize much or all of the available organic matter. Ironically, this expanding habitat was not conducive to providing a good fossil record. The whole fossil record is controlled by what preservation has allowed, but the Mesoproterozoic record may have a distinct bias as a result of the global rise in sulphate.

We acknowledge the Australian Microscopy & Microanalysis Research Facility at the Centre for Microscopy, Characterisation and Analysis, The University of Western Australia, a facility funded by the University, State and Commonwealth Governments. DW acknowledges funding from the European Commission and the Australian

Research Council. This is publication number 838 from the Australian Research Council Centre of Excellence for Core to Crust Fluid Systems.

References

Andrews, S.D., Trewin, N.H., Hartley, A.J. & Weedon, G.P. 2010. Solar variance recorded in lacustrine deposits from the Devonian and Proterozoic of Scotland. *Journal of the Geological Society, London*, **167**, 847–856, https://doi.org/10.1144/0016-76492009-105

Battison, L. & Brasier, M.D. 2012. Remarkably preserved prokaryote and eukaryote microfossils within 1 Ga-old lake phosphates of the Torridon Group, NW Scotland. *Precambrian Research*, **196–197**, 204–217.

Blank, C.E. 2013. Origin and early evolution of photosynthetic eukaryotes in freshwater environments – reinterpreting Proterozoic paleobiology and biogeochemical processes in light of trait evolution. *Journal of Phycology*, **49**, 1040–1055.

Brabec, M.Y., Lyons, T.W. & Mandernack, K.W. 2012. Oxygen and sulphur isotope fractionation during sulphide oxidation by anoxygenic phototrophic bacteria. *Geochimica et Cosmochimica Acta*, **83**, 234–251.

Briggs, D.E.G., Bottrell, S.H. & Raiswell, R. 1991. Pyritization of soft-bodied fossils: Beecher's trilobite bed, Upper Ordovician, New York State. *Geology*, **19**, 1221–1224.

Briggs, D.E.G., Raiswell, R., Bottrell, S.H., Hatfield, D. & Bartels, C. 1996. Controls on the pyritization of exceptionally preserved fossils: an analysis of the Lower Devonian Hunsrück Slate of Germany. *American Journal of Science*, **296**, 633–663.

Brydson, R. 2001. *Electron Energy Loss Spectroscopy*. Springer, New York.

Butterfield, N.J. 2015. Early evolution of the Eukaryota. *Palaeontology*, **58**, 5–17.

Canfield, D.E. & Farquhar, J. 2009. Animal evolution, bioturbation, and the sulfate concentration of the oceans. *Proceedings of the National Academy of Sciences*, **106**, 8123–8127.

Canfield, D.E., Raiswell, R., Westrich, J.T., Reaves, C.M. & Berner, R.A. 1986. The use of chromium reduction in the analysis of reduced inorganic sulphur in sediments and shale. *Chemical Geology*, **54**, 149–155.

Cawood, P.A., Nemchin, A.A., Strachan, R., Prave, T. & Krabbendam, M. 2007. Sedimentary basin and detrital zircon record along East Laurentia and Baltica during assembly and breakup of Rodinia. *Journal of the Geological Society, London*, **164**, 257–275, https://doi.org/10.1144/0016-76492006-115

Cloud, P. & Germs, A. 1971. New Pre-Paleozoic nannofossils from the Stoer Formation (Torridonian), northwest Scotland. *Geological Society of America Bulletin*, **82**, 3469–3474.

Cohen, P.A. & MacDonald, F.A. 2015. The Proterozoic record of eukaryotes. *Paleobiology*, **41**, 610–632.

Eme, L., Sharpe, S.C., Brown, M.W. & Roger, A.J. 2014. On the age of eukaryotes: evaluating evidence from fossils and molecular clocks. *Cold Spring Harbor Perspectives in Biology*, **6**, https://doi.org/10.1101/cshperspect.a016139

Farquhar, J., Cliff, J. *et al.* 2013. Pathways for Neoarchean pyrite formation constrained by mass-independent sulfur isotopes. *Proceedings of the National Academy of Sciences*, **110**, 17638–17643.

Kah, L.C., Lyons, T.W. & Frank, T.D. 2004. Low marine sulphate and protracted oxygenation of the Proterozoic biosphere. *Nature*, **431**, 834–838.

Knoll, A.H., Worndle, S. & Kah, L.C. 2013. Covariance of microfossil assemblages and microbialite textures across an Upper Mesoproterozoic carbonate platform. *Palaios*, **28**, 453–470.

Krevs, A. & Kucinskiene, A. 2012. Microbial decomposition of organic matter in the bottom sediments of small lakes of the urban landscape (Lithuania). *Microbiology*, **81**, 477–483.

Lamb, D.M., Awramik, S.M., Chapman, D.J. & Zhu, S. 2009. Evidence for eukaryotic diversification in the *c.* 1800 million-year-old Changzhougou Formation, North China. *Precambrian Research*, **173**, 93–104.

Lyons, T.W., Reinhard, C.T., Love, G.D. & Xiao, S. 2012. Geobiology of the Proterozoic Eon. *In*: Knoll, A.H., Canfield, D.E. & Konhauser, K.O. (eds) *Fundamentals of Geobiology*. Wiley, New York.

Muir, M.D. 1976. Proterozoic microfossils from the Amelia Dolomite, McArthur Basin, Northern Territory. *Alcheringa*, **1**, 143–158.

Parnell, J., Boyce, A.J., Mark, D., Bowden, S. & Spinks, S. 2010. Early oxygenation of the terrestrial environment during the Mesoproterozoic. *Nature*, **468**, 290–293.

Parnell, J., Mark, D., Fallick, A.E., Boyce, A. & Thackrey, S. 2011. The age of the Mesoproterozoic Stoer Group sedimentary and impact deposits, NW Scotland. *Journal of the Geological Society, London*, **168**, 349–358, https://doi.org/10.1144/0016-76492010-099

Parnell, J., Still, J., Spinks, S., Thayalan, W. & Bowden, S. 2014. Cadmium sulfide in a Mesoproterozoic terrestrial environment. *Mineralogical Magazine*, **78**, 47–54.

Parnell, J., Spinks, S., Andrews, S., Thayalon, W. & Bowden, S. 2015. High molybdenum availability for evolution in a Mesoproterozoic lacustrine environment. *Nature Communications*, **6**, https://doi.org/10.1038/ncomms7996

Porter, S.M. & Knoll, A.H. 2000. Testate amoebae in the Neoproterozoic Era: evidence from vase-shaped microfossils in the Chuar Group, Grand Canyon. *Paleobiology*, **26**, 360–385.

Robinson, B.W. & Kusakabe, M. 1975. Quantitative preparation of SO_2 for $^{34}S/^{32}S$ analysis from sulfides by combustion with cuprous oxide. *Analytical Chemistry*, **47**, 1179–1181.

Sagemann, J., Bale, S.J., Briggs, D.E.G. & Parkes, R.J. 1999. Controls on the formation of authigenic minerals in association with decaying organic matter: an experimental approach. *Geochimica et Cosmochimica Acta*, **63**, 1083–1095.

Schiffbauer, J.D., Xiao, S. *et al.* 2014. A unifying model for Neoproterozoic–Palaeozoic exceptional

fossil preservation through pyritization and carbonaceous compression. *Nature Communications*, **5**, https://doi.org/10.1038/ncomms6754

Spinks, S.C., Parnell, J., Bowden, S., Taylor, R.A.D. & MacLean, M.E. 2014. Enhanced organic carbon burial in large Proterozoic lakes: implications for atmospheric oxygenation. *Precambrian Research*, **255**, 202–215.

Stewart, A.D. 2002. *The Later Proterozoic Torridonian Rocks of Scotland: Their Sedimentology, Geochemistry and Origin*. Geological Society, London, Memoirs, **24**, http://mem.lyellcollection.org/content/24/1.toc

Strother, P.K., Battison, L., Brasier, M.D. & Wellman, C.H. 2011. Earth's earliest non-marine eukaryotes. *Nature*, **473**, 505–509.

Tang, D., Shi, X., Jiang, G., Pei, Y. & Zhang, W. 2013. Environment controls on Mesoproterozoic thrombolite morphogenesis: a case study from the North China Platform. *Journal of Palaeogeography*, **2**, 275–296.

Turnbull, M.J.M., Whitehouse, M.J. & Moorbath, S. 1996. New isotopic age determinations for the Torridonian, NW Scotland. *Journal of the Geological Society, London*, **153**, 955–964, https://doi.org/10.1144/gsjgs.153.6.0955

Wacey, D., Kilburn, M.R., Saunders, M., Cliff, J. & Brasier, M.D. 2011. Microfossils of sulphur-metabolizing cells in 3.4 billion-year-old rocks of Western Australia. *Nature Geoscience*, **4**, 698–702.

Wacey, D., Menon, S. *et al.* 2012. Taphonomy of very ancient microfossils from the *c.* 3400 Ma Strelley Pool Formation and *c.* 1900 Ma Gunflint Formation: new insights using focused ion beam. *Precambrian Research*, **220–221**, 234–250.

Wacey, D., McLoughlin, N. *et al.* 2013. Nanoscale analysis of pyritized microfossils reveals differential heterotrophic consumption in the *c.* 1.9-Ga Gunflint chert. *Proceedings of the National Academy of Sciences of the United States of America*, **110**, 8020–8024.

Wacey, D., Saunders, M. *et al.* 2014. Enhanced cellular preservation by clay minerals in 1 billion year-old lakes. *Scientific Reports*, **4**, https://doi.org/10.1038/srep05841

Warren, J.K. 2010. Evaporites through time: tectonic, climatic and eustatic controls in marine and nonmarine deposits. *Earth-Science Reviews*, **98**, 217–268.

Wellman, C.H. & Strother, P.K. 2015. The terrestrial biota prior to the origin of land plants (embryophytes): a review of the evidence. *Palaeontology*, **58**, 601–627.

Westrich, J.T. & Berner, R.A. 1984. The role of sedimentary organic matter in bacterial sulphate reduction: the G model tested. *Limnology and Oceanography*, **29**, 236–249.